

First simultaneous $K^- p \rightarrow \Sigma^0 \pi^0, \Lambda \pi^0$ cross section measurements at 98 MeV/c

Kristian Piscicchia,^{1,2} Magdalena Skurzok^{1b,3,4,*} Michael Cargnelli,⁵ Raffaele Del Grande,^{6,2} Laura Fabbietti,^{6,7} Johann Marton,⁵ Pawel Moskal,^{3,4} Àngels Ramos,⁸ Alessandro Scordo,² Diana Laura Sirghi,^{2,9,1} Oton Vazquez Doce,² Johann Zmeskal,^{2,5} Sławomir Wycech,¹⁰ Paolo Branchini,¹¹ Filippo Ceradini,^{12,11} Eryk Czerwiński,^{3,4} Erika De Lucia,² Salvatore Fiore,^{13,14} Andrzej Kupsc,^{15,10} Giuseppe Mandaglio,^{16,17} Matteo Martini,^{2,18} Antonio Passeri,¹¹ Vincenzo Patera,^{14,19} Elena Perez Del Rio,^{3,4} Andrea Selce,^{12,11} Michał Silarski,^{3,4} and Catalina Curceanu²

¹Centro Ricerche Enrico Fermi - Museo Storico della Fisica e Centro Studi e Ricerche “Enrico Fermi”, 00184 Rome, Italy, EU

²INFN (Istituto Nazionale di Fisica Nucleare) —Laboratori Nazionali di Frascati, 00044 Frascati, Italy, EU

³Marian Smoluchowski Institute of Physics, Jagiellonian University, 30348 Cracow, Poland, EU

⁴Center for Theranostics, Jagiellonian University, 31034 Cracow, Poland, EU

⁵Stefan-Meyer-Institute for Subatomic Physics, Austrian Academy of Science, 1090 Wien, Austria, EU

⁶Physik Department E62, Technische Universität München, 85748 Garching, Germany, EU

⁷Excellence Cluster “Origin and Structure of the Universe”, 85748 Garching, Germany, EU

⁸Facultat de Física, Universitat de Barcelona, 08028 Barcelona, Spain, EU

⁹IFIN-HH, Institutul National pentru Fizica si Inginerie Nucleara Horia Hulubei, 077125 Măgurele, Romania, EU

¹⁰National Centre for Nuclear Research, 00681 Warsaw, Poland, EU

¹¹INFN - Istituto Nazionale di Fisica Nucleare Sezione di Roma Tre, 00146 Roma, Italy, EU

¹²Dipartimento di Matematica e Fisica dell’Università “Roma Tre”, 00146 Roma, Italy, EU

¹³ENEA, Department of Fusion and Technology for Nuclear Safety and Security, 00044 Frascati (Rome), Italy, EU

¹⁴INFN - Istituto Nazionale di Fisica Nucleare Sezione di Roma, 00185 Roma, Italy, EU

¹⁵Department of Physics and Astronomy, Uppsala University, 751 20 Uppsala, Sweden, EU

¹⁶Dipartimento di Scienze Matematiche e Informatiche, Scienze Fisiche e Scienze della Terra dell’Università di Messina, 98122 Messina, Italy, EU

¹⁷INFN - Istituto Nazionale di Fisica Nucleare Sezione di Catania, 95123 Catania, Italy, EU

¹⁸Dipartimento di Scienze e Tecnologie applicate, Università “Guglielmo Marconi”, 00193 Roma, Italy, EU

¹⁹Dipartimento di Scienze di Base ed Applicate per l’Ingegneria dell’Università “Sapienza”, 00185 Roma, Italy, EU



(Received 9 November 2022; accepted 8 September 2023; published 6 November 2023)

Simultaneous measurements of the $K^- p \rightarrow \Sigma^0 \pi^0$ and $K^- p \rightarrow \Lambda \pi^0$ cross sections below 100 MeV/c kaon momentum have been performed. The kaon beam delivered by the DAΦNE collider was exploited to detect K^- absorptions on hydrogen atoms populating the gas mixture of the KLOE drift chamber. The cross sections are determined with the highest yet obtained precision in the low kaon momentum regime [$\sigma_{K^- p \rightarrow \Sigma^0 \pi^0} = 42.8 \pm 1.5(\text{stat})_{-2.0}^{+2.4}(\text{syst})$ mb and $\sigma_{K^- p \rightarrow \Lambda \pi^0} = 31.0 \pm 0.5(\text{stat})_{-1.2}^{+1.2}(\text{syst})$ mb] impacting on pending questions in several fields, ranging from nuclear and particle physics, to astrophysics.

DOI: [10.1103/PhysRevC.108.055201](https://doi.org/10.1103/PhysRevC.108.055201)

I. INTRODUCTION

The present work provides precision cross section measurements in the neutral meson-baryon sector with strangeness $S = -1$. This is the closest to the $\bar{K}N$ threshold and a simultaneous and independent measurement of the isospin $I = 0$ and $I = 1$ cross sections, hence boosting our understanding of the meson-baryon interaction at low energies, which is a crucial ingredient to comprehend several interesting phenomena in various fields of research.

Presently, the available data for the inelastic $K^- p \rightarrow \Sigma^0 \pi^0$ cross section close to threshold are obtained by means of indirect extrapolations, in bubble chamber experiments [1,2], from the measurements in the $\Lambda \pi^0$ channel, by ex-

ploiting isospin symmetry. Three cross sections are given at mean kaon momenta $p_{K^-} = 120, 160,$ and 200 MeV/c, which are affected by sizable relative errors (as large as 50% at $p_{K^-} = 120$ MeV/c), the p_{K^-} momentum intervals around the central values being 25 MeV/c wide.

This work takes advantage of the low momentum negative kaons beam produced at the DAΦNE e^+e^- collider [3], which delivers almost monochromatic charged kaons with $p_{K^-} \approx 127$ MeV/c. The gas filling the drift chamber of the KLOE [4] spectrometer is used as an active target. In order to disentangle in-flight K^- absorptions on hydrogen in the gas mixture of the KLOE drift chamber [5], a complete characterization of all possible nuclear absorption reactions was achieved. This allowed the first simultaneous and independent measurement of the $K^- p \rightarrow (\Sigma^0/\Lambda) \pi^0$ cross sections, with greatly improved precision with respect to other available (indirect) measurements, at the lowest energy ever ($p_{K^-} = 98 \pm 10$ MeV/c).

*magdalena.skurzok@uj.edu.pl

The simultaneous measurement of the $I = 0$ and $I = 1$ cross sections, considerably closer to the $\bar{K}N$ threshold, will allow to precisely pin down the K^-p and K^-n scattering amplitudes below the threshold. While all recent chiral models give a rather similar description of the K^-p scattering length (thanks to the precise SIDDHARTA measurement [6]), the subthreshold elastic and inelastic amplitudes differ by factors of three or more [7].

A proper comprehension of the subthreshold $\bar{K}N$ amplitudes will sizably reduce the uncertainty in the $\Lambda(1405)$ pole [8], thus strongly contributing to a solution of this puzzle. The $\Lambda(1405)$ has, since its discovery, eluded a proper description in terms of quark models. It is presently consolidating as an exotic resonant structure in a coupled-channel formulation of the $\bar{K}N$ interaction, more than 50 years after its prediction [9,10]. This picture finds support in the two-pole structure predicted for this state by all coupled-channel unitarized models [11–18], which would also explain the observed dependence of the spectral shapes on the production mechanism and measured decay channels [19–23]. The discovery by LHCb of the $P_c(4312)^+$ and $P_c(4450)^+$ pentaquarks [24,25], and the suggested tetraquark nature for the $Z_c(3900)$ state seen at BESIII and Belle [26,27], have triggered a lot of activity in the search of exotic mesons and baryons. Their interpretation as compact multi-quark objects or as molecular systems ultimately relies on a deep understanding of the dynamics of their constituents (see, e.g., [28–34]). In this respect, a more precise knowledge of the $\bar{K}N$ interaction will serve to better constrain the models employed to confront lattice quantum chromodynamics (QCD) simulations of the low lying odd-parity Λ spectrum [35–38], as well as guiding future studies of $S = -1$ meson-baryon systems in the all-to-all quark propagator technique (where the $S = 1$ sector [39] and coupled channel approaches [40] were explored), hence moving towards a final answer as to the long-sought nature of the $\Lambda(1405)$ and also contributing to one of the many expected lattice QCD developments in the low energy regime [41].

Hadron interactions at low and subthreshold energies have an impact in several other fields. The search for exotic mesic (kaonic, η , η') nuclear bound states [42–48] and the interpretation of the big amount of contradicting experimental findings on \bar{K} -multi- N bound states (see [49–61] and references therein) greatly benefit from a subthreshold extrapolation of the $\bar{K}N$ interaction with reduced uncertainties. The size of the strong attraction in the $\bar{K}N$ $I = 0$ channel critically influences the debated shrinkage effect of bound $\Lambda(1405)$ -matter systems, a dark matter component conjectured to be formed during the Big Bang quark gluon plasma period in the early universe [62–64]. The properties of (anti)kaons in dense nuclear matter are investigated in heavy-ion and proton-nuclei collisions. The data are interpreted by means of transport models and collision calculations, which require precise knowledge of the low-energy K^- -nucleon cross sections [65–67]. Finally, combination of astrophysical and heavy-ion collisions data is providing new constraints on neutron star matter [68], hence providing an improved framework to elucidate whether strange hadrons, such as kaons or hyperons, may appear in neutron stars, which is a hot topic in astrophysics, as their presence influences the structure and

dynamical evolution of those dense stellar objects (see, e.g., [69–76] and references therein). The precise knowledge of the interactions of strange hadrons is fundamental to determine, for instance, whether it is possible to reconcile the presence of kaon condensation or hyperons in the neutron star interiors with the recent observations of millisecond pulsars with unusually large masses [77–79]. Our data provide basic information to develop realistic models of nuclear dynamics at the core of compact objects.

II. DATA SAMPLE

In this work a total integrated luminosity of 1.74 fb^{-1} , corresponding to the 2004/2005 KLOE data taking campaign, was analyzed by the AMADEUS collaboration. The KLOE detector is centered around the DAΦNE interaction point and consists of a large cylindrical drift chamber (DC), for tracking analysis, and a fine sampling lead-scintillating fibers calorimeter [80], used in this study to determine position, time, and energy of the ionization deposits in the fibers caused by particles hitting the calorimeter (clusters), all immersed in the axial magnetic field of a superconducting solenoid (0.52 T). The DC is filled with a mixture of helium and isobutane C_4H_{10} (90% of helium and 10% of isobutane in volume). For more details on the DC and calorimeter performances and resolutions we refer to [5,80]. The strategy for the measurement of the $K^-p \rightarrow \Sigma^0\pi^0$ and $K^-p \rightarrow \Lambda\pi^0$ cross sections consists in the identification of K^- absorptions in-flight on the hydrogen atoms of the isobutane molecules.

III. EVENTS SELECTION

The identification of a $\Lambda(1116)$ hyperon, through its decay into a proton and a negatively charged pion [$\text{BR}_{\Lambda \rightarrow p\pi^-} = (63.9 \pm 0.5)\%$] [81] represents the signature of a hadronic interaction and the starting point of this analysis. Protons and pions are selected by combining dE/dx (truncated mean of the analog to digital converter (ADC) counts due to ionization in the DC gas) versus momentum information, with the measurement of the clusters energies, as described in Refs. [60,82]. K^- nuclear absorptions in the gas filling the DC volume are sorted by requiring the radial distance of the Λ decay vertex from the DAΦNE beam pipe axis (ρ_Λ) to be greater than 30 cm. The cut is optimized based on Monte Carlo (MC) simulations [performed by means of the standard KLOE GEANT digitization (GEANFI [83])], in order to minimize the contamination with K^- absorptions in the DC entrance wall (aluminated carbon fiber), which amounts to less than 3% for the selected sample.

The events selection proceeds through the photons identification by time of flight. Following the convention $\pi^0 \rightarrow \gamma_1\gamma_2$ and $\Sigma^0 \rightarrow \Lambda\gamma_3$, for the two channels under study, the two (or three) neutral clusters in the calorimeter (characterized by energy $E > 20 \text{ MeV}$, no associated track, and not produced in a K^+ decay) are first selected by minimizing a time of flight based χ_t^2 variable. Further, the photons are associated to the π^0 (and to the Σ^0) by a second χ_m^2 analysis, using the $m_{\gamma_1\gamma_2}$ or the combined $m_{\gamma_1\gamma_2}$ and $m_{\Lambda\gamma_3}$ invariant masses information, respectively. The constraints $\chi_t^2 < 20$, $\chi_{m_{\gamma_1\gamma_2}}^2 < 5$, and

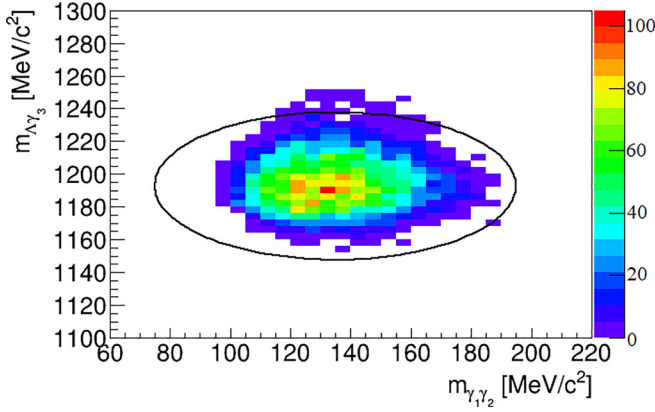


FIG. 1. The plot shows the $m_{\Lambda\gamma_3}$ distribution as a function of $m_{\gamma_1\gamma_2}$. A black ellipse represents the applied selection in the two invariant masses space.

$\chi^2_{m_{\Lambda\gamma_3}} < 4$ are tuned based on MC studies. A check against cluster splitting (single clusters in the calorimeter erroneously recognized as two clusters) is performed by analyzing the clusters distance as a function of energy (see Ref. [82]). The selected sample is not significantly affected by splitting. The algorithm's efficiency for the photons clusters recognition is 0.98 ± 0.01 [82].

In Fig. 1 $m_{\Lambda\gamma_3}$ is represented as a function of $m_{\gamma_1\gamma_2}$. Gaussian fits to the invariant mass distributions yield the resolutions $\sigma_{\gamma_1\gamma_2} \approx 20$ MeV/c and $\sigma_{\Lambda\gamma_3} \approx 15$ MeV/c, respectively. Accordingly the following additional cuts are applied for the two channels: $(m_{\Lambda\gamma_3} - m_{\Sigma^0})^2 / (3\sigma_{\Lambda\gamma_3})^2 + (m_{\gamma_1\gamma_2} - m_{\pi^0})^2 / (3\sigma_{\gamma_1\gamma_2})^2 < 1$ and $|m_{\gamma_1\gamma_2} - m_{\pi^0}| < 3\sigma_{\gamma_1\gamma_2}$.

The optimization of the following phase space selections is aimed to disentangle the signal processes ($K^-H \rightarrow (\Sigma^0/\Lambda)\pi^0$ absorptions in flight) from the competing background reactions, taking advantage of the signal's distinctive kinematics. This requires simulations of the involved reactions, which also serve for the data fit.

When a negative kaon is absorbed in the DC gas, the final state $\Sigma^0\pi^0$ can be produced in $K^- + H \rightarrow \Sigma^0 + \pi^0$ at rest (*ar*) or in flight (*if*), or due to K^- absorption on a bound proton in ${}^4\text{He}$ or ${}^{12}\text{C}$, *ar* or *if*. Analogous reactions also give rise to the $\Lambda\pi^0$ production both in direct processes ($K^-p \rightarrow \Lambda\pi^0$) or as a result of a Σ^0 decay ($K^-p \rightarrow \Sigma^0\pi^0 \rightarrow \Lambda\gamma\pi^0$). Besides the direct processes and Σ^0 decay, in the nucleus also elastic or inelastic final state interactions (FSI) can end up with the observed hyperon ($Y = \Sigma^0, \Lambda$) and π^0 . After phase space selections the contribution of the FSI is minor, and will be considered in the evaluation of the systematic uncertainties.

The case of K^- absorption on H is straightforward, since the kinematics is determined by energy-momentum conservation, for both *ar* and *if*. Calculation of the *if* reaction requires as input the negative kaon momentum, which is sampled according to the true MC (i.e., not passed for events reconstruction) momentum distribution of the negative kaons inside the DC volume. The simulations of the K^- nuclear absorption processes are performed according to a phenomenological model (see Refs. [84–86]) which provides, for each reaction, the total hyperon-pion momentum probability distribution

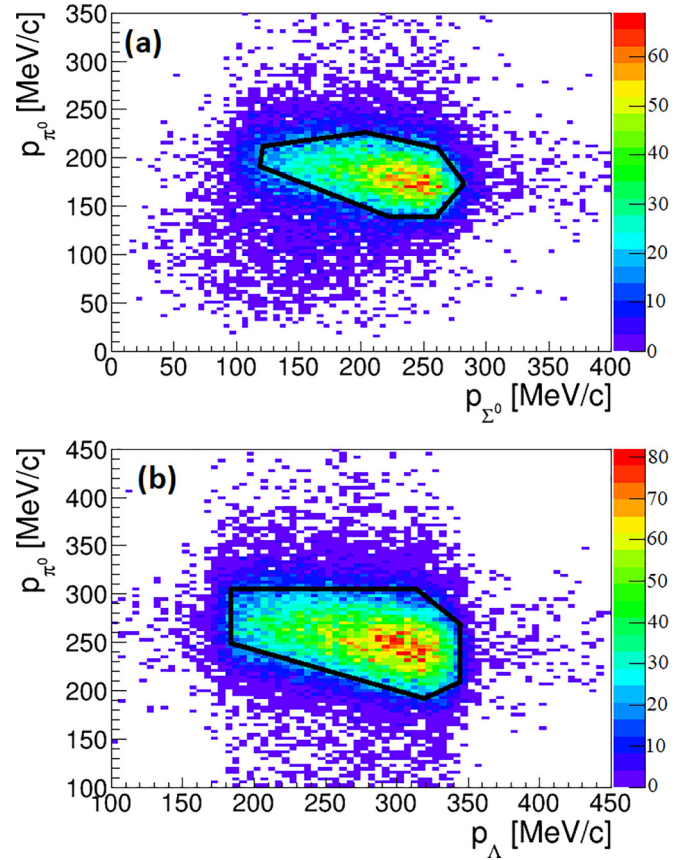


FIG. 2. The plot shows reconstructed MC p_{π^0} vs. p_Y distributions for the $K^-H \rightarrow \Sigma^0\pi^0$ *if* reaction (top) and $K^-H \rightarrow \Lambda\pi^0$ *if* reaction (bottom). The phase space selections are represented as black contours.

$P(p_Y\pi^0)$. The kinematics of an event is completely defined by the momentum vectors $(\mathbf{p}_Y, \mathbf{p}_{\pi^0})$ [the residual(s) nucleus track(s) is not detected], which are generated by sampling the $P(p_Y\pi^0)$ distribution, and applying energy and momentum conservation. For each event the calculated $(\mathbf{p}_Y, \mathbf{p}_{\pi^0})$ pairs represent the input for the KLOE GEANT digitization, followed by the event reconstruction.

The $K^-H \rightarrow (\Sigma^0/\Lambda)\pi^0$ *if* signal is characterized by an almost back-to-back production of the emerging $Y - \pi^0$. We use this feature to enhance the signal over background ratio. In Fig. 2 (top) and (bottom) the reconstructed MC p_{π^0} versus p_Y distributions are shown, for signal events in the $\Sigma^0\pi^0$ and $\Lambda\pi^0$ channels, respectively. The simulations are used to optimize two-dimensional cuts, which are represented in Fig. 2 as black contours. Additionally, thanks to the good resolution in the Λ momentum ($\sigma_{p_\Lambda} \approx 1.9$ MeV/c for Λ s produced in the DC gas [82]), $K^-H \rightarrow \Lambda\pi^0$ (*ar* and *if*) events can be effectively sampled as they are characterized by the sharp angular correlation $\cos\theta_{\Lambda\pi^0} < -0.85$ (where $\theta_{\Lambda\pi^0}$ is the angle between the two particles momentum vectors). Hence, this additional condition is set for the $\Lambda\pi^0$ sample.

Panels (a) in Figs. 3 and 4 exemplify the core of the final analysis step. Due to momentum conservation, the total hyperon-pion momentum ($p_{Y\pi^0}$) distributions of the $K^-H \rightarrow Y\pi^0$ *if* samples reflect the original K^- momentum spectrum,

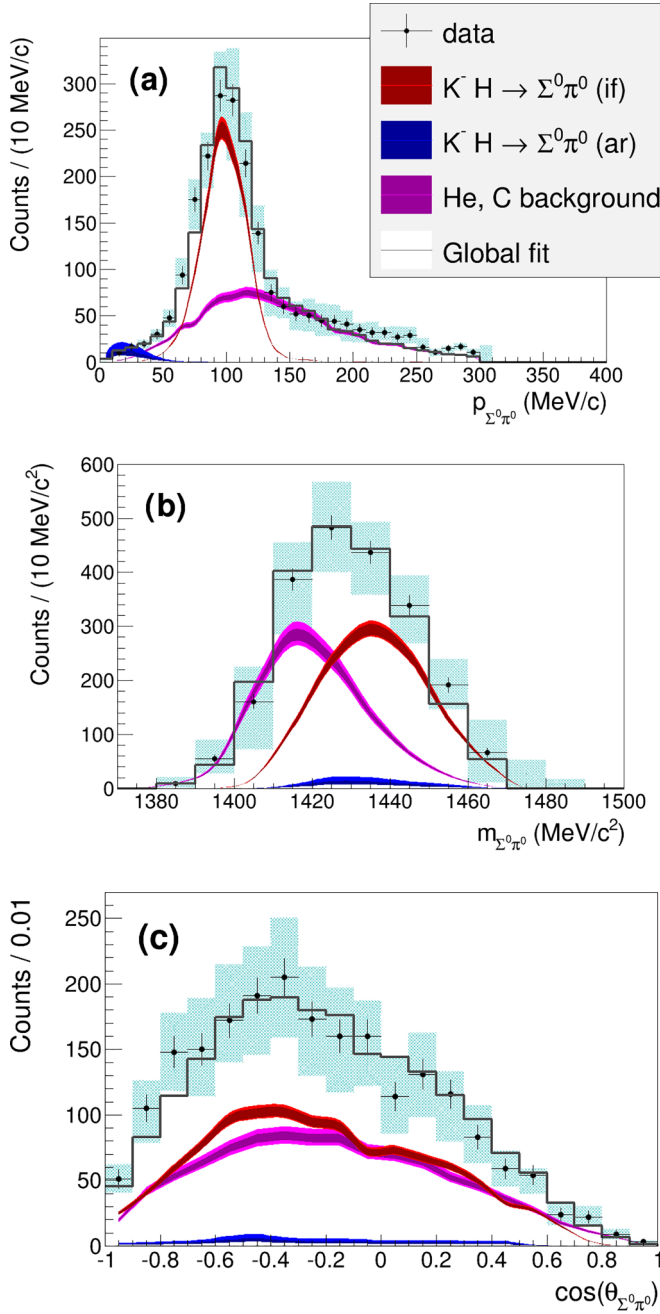


FIG. 3. From top to bottom the figure shows the result of the simultaneous fit of $p_{\Sigma^0\pi^0}$, $m_{\Sigma^0\pi^0}$, and $\cos\theta_{\Sigma^0\pi^0}$. The experimental data and the corresponding statistical errors are represented by black crosses, the systematic errors are light blue (gray) boxes. The contributions of the various physical processes are shown as colored histograms, according to the color code shown in the caption. The light and dark bands correspond to systematic and statistical errors, respectively. The gray (solid) distribution reproduces the global fit function.

as demonstrated by the preminent peaks centered at $p_{Y\pi^0} \approx 98$ MeV/c. This hallmark allows to efficiently disentangle the remaining background due to the competing K^- absorption processes.

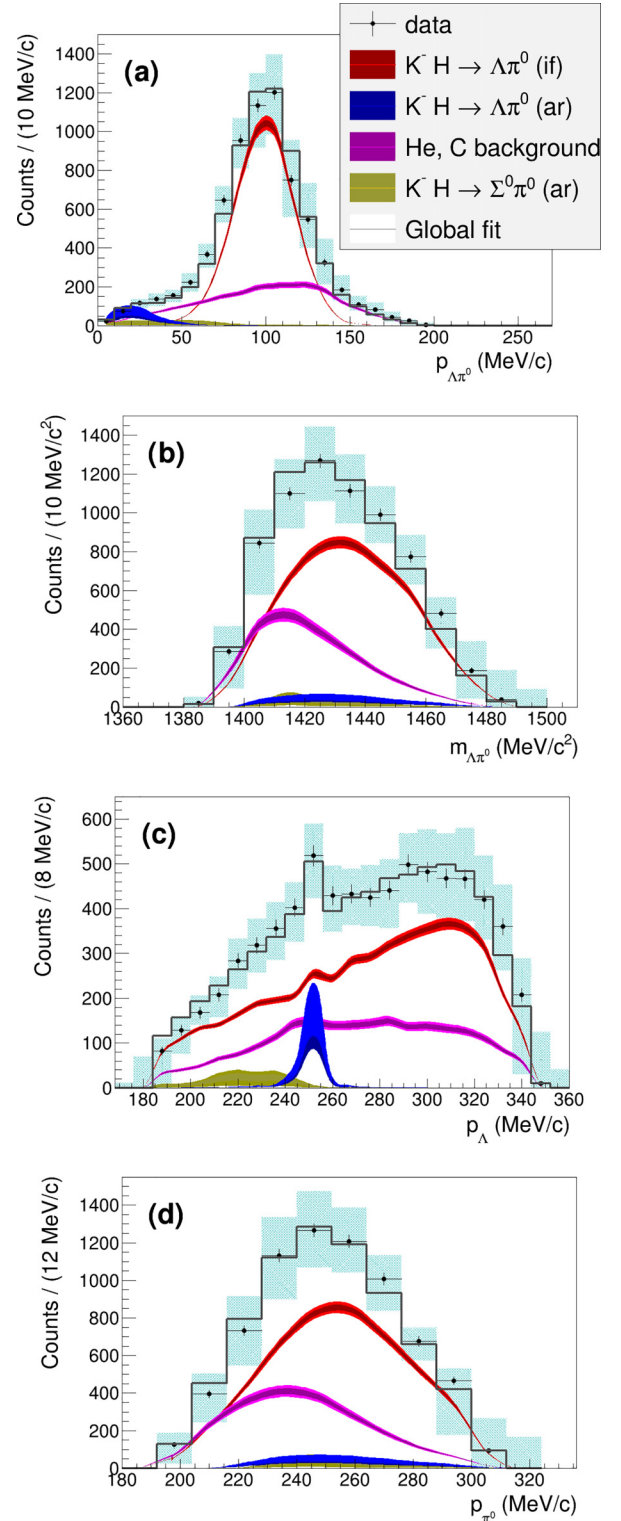


FIG. 4. From top to bottom the figure shows the result of the simultaneous fit of $p_{\Lambda\pi^0}$, $m_{\Lambda\pi^0}$, p_{Λ} , and p_{π^0} . The experimental data and the corresponding statistical errors are represented by black crosses, the systematic errors are light blue boxes. The contributions of the various physical processes are shown as colored histograms, according to the color code shown in the caption. The light and dark bands correspond to systematic and statistical errors, respectively. The gray distribution reproduces the global fit function.

At this stage of the events selection 6.5% of the $\Sigma^0\pi^0$ events lie in the $p_{\Sigma^0\pi^0} > 300$ MeV/c region, a phase space sector far away from the region of interest, mainly populated by FSI processes (see, e.g., Ref. [86]). A final phase space selection $p_{\Sigma^0\pi^0} < 300$ MeV/c is then applied.

The selected $\Sigma^0\pi^0$ and $\Lambda\pi^0$ samples amount to 2130 and 7106 events, respectively.

IV. $K^-p \rightarrow (\Sigma^0/\Lambda)\pi^0$ CROSS SECTIONS DETERMINATION

The data are fitted by minimizing the following χ^2 function:

$$\chi^2 = \sum_q \sum_{n=1}^{N_{bins}^q} \frac{(N_n^q - \mathcal{F}^q(q_n))^2}{\sigma_n^{q2}}, \quad (1)$$

in which q ranges over the observables, n over the number of bins of the q th spectrum and N_n^q is the measured content of the corresponding n th bin. The fit function \mathcal{F} contains the following physical processes (with the color code adopted in Figs. 3 and 4):

- (1) $K^-H \rightarrow (\Sigma^0/\Lambda)\pi^0$ *if* (red),
- (2) $K^-H \rightarrow (\Sigma^0/\Lambda)\pi^0$ *ar* (blue),
- (3) $K^- + {}^4\text{He}/{}^{12}\text{C} \rightarrow \Sigma^0/\Lambda + \pi^0 + {}^3\text{H}/{}^{11}\text{B}$ (magenta).

In Ref. [86] equivalent contributions are measured, within the uncertainties, for K^- absorptions on ${}^4\text{He}$ and ${}^{12}\text{C}$ nuclei in the DC gas, as well as for the competing in-flight and at-rest nuclear interactions of the negative kaon. Accordingly, component 3 is prepared as an equal weight cocktail of the mentioned reactions and the related uncertainty is considered as a systematic effect. For the $\Lambda\pi^0$ channel, besides the direct processes 1–3, \mathcal{F} also accounts for the same reactions initiated by $\Sigma^0\pi^0$ production and followed by $\Sigma^0 \rightarrow \Lambda\gamma$ decay.

\mathcal{F} is given by the linear combination

$$\mathcal{F}^q(q_n) = \sum_{i=1}^{N_{par}} \alpha_i \cdot h_i^q(q_n) \quad (2)$$

with the index i running over the number of free parameters α_i and h_i^q representing the distribution of the observable q , for the i th physical process, normalized to the data entries. In Eq. (1) the errors are evaluated as $\sigma_n^{q2} = \sqrt{\sum_{i=1}^{N_{par}} (\alpha_i \cdot h_i^q(q_n))^2 + N_n^q}$ and the χ^2 function minimization is performed by means of the SIMPLEX, MIGRAD, and MINOS routines of ROOT [87].

For the $\Sigma^0\pi^0$ sample a simultaneous fit is performed over $q = m_{\Sigma^0\pi^0}, \cos\theta_{\Sigma^0\pi^0}, p_{\Sigma^0\pi^0}$, which indicate the $\Sigma^0\pi^0$ invariant mass, angular correlation, and total momentum, respectively. In the $\Lambda\pi^0$ channel the sharp selection of back-to-back events renders the $\cos\theta_{\Lambda\pi^0}$ variable insensitive to the uncorrelated K^- nuclear absorption reactions, hence the (kinematically equivalent) combination $q = m_{\Lambda\pi^0}, p_{\Lambda}, p_{\pi^0}, p_{\Lambda\pi^0}$ is chosen. The fits results are presented in Figs. 3 (for $\Sigma^0\pi^0$) and 4 (for $\Lambda\pi^0$) and the obtained parameters values are summarized in Table I.

TABLE I. The table summarizes the reduced χ -squares and the fit parameters obtained from the fits of the $\Sigma^0\pi^0$ and $\Lambda\pi^0$ samples.

$\Sigma^0 - \pi^0$ channel ($\frac{\chi^2}{dof} = \frac{92}{54}$)	fit par.	$\sigma_{stat.}$
$K^-H \rightarrow \Sigma^0\pi^0$ (<i>if</i>)	0.511	± 0.018
$K^-H \rightarrow \Sigma^0\pi^0$ (<i>ar</i>)	0.017	± 0.005
$K^- + {}^4\text{He}/{}^{12}\text{C} \rightarrow \Sigma^0\pi^0 + \text{residual}$ (<i>ar/if</i>)	0.463	± 0.018
$\Lambda - \pi^0$ channel ($\frac{\chi^2}{dof} = \frac{165}{57}$)	fit par.	$\sigma_{stat.}$
$K^-H \rightarrow \Lambda\pi^0$ (<i>if</i>)	0.659	± 0.011
$K^-H \rightarrow \Lambda\pi^0$ (<i>ar</i>)	0.021	± 0.003
$K^- + {}^4\text{He}/{}^{12}\text{C} \rightarrow \Lambda\pi^0 + \text{residual}$ (<i>ar/if</i>)	0.298	± 0.012
$K^-H \rightarrow \Sigma^0\pi^0 \rightarrow \Lambda\gamma\pi^0$ (<i>ar</i>)	0.018	± 0.006

The fit is not sensitive to the $\Lambda\pi^0$ kinematic distributions originated in Σ^0 decays, for the K^-H interaction (*if*) and the nuclear K^- absorptions, it yields negligibly small contributions which are set to zero in the final fit.

The cross sections are calculated in accordance with

$$\sigma = \frac{N_{K^-p \rightarrow Y\pi^0}^{if}}{N_{K^-} \cdot n \cdot L}, \quad (3)$$

where the total number of expected signal events $N_{K^-p \rightarrow Y\pi^0}^{if}$ is obtained rescaling for the detection and reconstruction efficiencies and for the branching ratio of the $\Lambda \rightarrow p\pi^-$ decay. Normalization to an absolute number of negative kaons is performed taking advantage of the K^+ tagging (see Refs. [60,61]). The number of projectiles N_{K^-} corresponds to the number of tagged kaons corrected for the decay, by means of a MC simulation following the K^- tracks (till the decay) in steps of 1 cm. n is the numerical density of hydrogen scattering centers. L is the effective mean path length, obtained through a MC simulation, accounting for the K^- impinging angle, i.e., the angle between the tangent vector to the particle trajectory at the DC entrance point, and the radial direction.

The obtained cross sections,

$$\sigma_{K^-p \rightarrow \Sigma^0\pi^0} = 42.8 \pm 1.5(\text{stat})_{-2.0}^{+2.4}(\text{syst}) \text{ mb}$$

$$\sigma_{K^-p \rightarrow \Lambda\pi^0} = 31.0 \pm 0.5(\text{stat})_{-1.2}^{+1.2}(\text{syst}) \text{ mb},$$

correspond to a mean kaon momentum $p_K = (98 \pm 10)$ MeV/c, calculated on the basis of the true MC information of the negative kaons momentum distribution inside the DC volume.

The systematic errors are determined by repeating several times the fit procedure, by varying independently all the analysis cuts which were optimized for the $\Sigma^0\pi^0$ and $\Lambda\pi^0$ samples selection. The systematic error on the i th parameter of the fit, due to a variation of the j th cut, is defined as

$$\sigma_{sist,i}^j = \alpha_i^j - \alpha_i. \quad (4)$$

Total positive and negative systematic errors are obtained by summing in quadrature the positive and negative systematic fluctuations.

With the exception of those quantities for which the statistical error is known (e.g., $m_{\gamma_1\gamma_2}$, $m_{\Lambda\gamma^3}$, and $\cos\theta_{\Lambda\pi^0}$), in which case the systematics are evaluated by applying 1σ fluctuations to the corresponding cuts, and of the background

sources whose contribution is known by simulations (e.g., the background introduced by the ρ_Λ cut), for the other selections we chose to change the cuts of the amount necessary to increase (or decrease) the selected number of events of 15% with respect to the standard. This is the case of the constraints on χ_i^2 , $\chi_{m_{\gamma_1\gamma_2}}^2$, and $\chi_{m_{\Lambda\gamma_3}}^2$, and of the phase space selections in the $p_{\pi^0} - p_{\Sigma^0}$ and in the $p_{\pi^0} - p_\Lambda$ planes. The systematic uncertainty introduced by setting equal contributions of K^- absorptions on helium and carbon, both for the *ar* and *if* processes, is set by performing 15% variations of the relative contribution of each process.

The $p_{\Sigma^0\pi^0}$ constraint was optimized based on a scan in the range (280–350) MeV/*c*, in steps of 10 MeV/*c* (compatible with the resolution $\sigma_{p_{\Sigma^0\pi^0}} \approx 15$ MeV/*c*) yielding the minimum reduced χ^2 for $p_{\Sigma^0\pi^0} = 300$ MeV/*c*. The contribution to the systematic errors is obtained by the condition $p_{\Sigma^0\pi^0} < 310$ MeV/*c*.

The systematics introduced by the decay correction in the N_K - calculation and by the evaluation of L are estimated by doubling the 1 cm step length, and diminishing of 15% the number of simulated kaons.

V. CONCLUSIONS

Concluding, an innovative technique was exploited to perform the simultaneous and independent measurement of the

$K^-p \rightarrow (\Sigma^0/\Lambda)\pi^0$ cross sections, at the lowest energy ever, by improving the relative errors of about one order of magnitude. The achieved precision, the narrower p_K -momentum range, and the closeness to the $\bar{K}N$ threshold, will significantly improve the theoretical models fit results [the analysis including AMADEUS data [8] (this article and [86]) resulted in 20% higher precision for $\Lambda(1405)$ resonance position determination]. Hence the K^-p and K^-n scattering amplitudes below the threshold, and resonances poles, will be precisely determined, leading to a solution of longstanding issues in hadron and nuclear physics and boosting the knowledge on hot sectors of particle physics and astrophysics.

ACKNOWLEDGMENTS

We acknowledge the KLOE/KLOE-2 Collaboration for their support and for having provided us with the data and the tools to perform the analysis presented in this paper. Part of this work was supported by the EU STRONG-2020 project (grant agreement no. 824093). The project is co-financed by the Polish National Agency for Academic Exchange, Grant no. PPN/BIT/2021/1/00037. Part of this work was supported by the Polish National Science Center through Grant No. 2016/21/D/ST2/01155.

-
- [1] W. E. Humphrey and R. R. Ross, *Phys. Rev.* **127**, 1305 (1962).
 - [2] J. K. Kim, Report No. Nevis-149, Columbia University, New York, 1966.
 - [3] A. Gallo *et al.*, Conf. Proc. C **060626**, 604 (2006).
 - [4] F. Bossi, E. DeLucia, J. Lee-Franzini, S. Miscetti, and M. Palutan, Riv. Nuovo Cim. **31**, 531 (2008).
 - [5] M. Adinolfi *et al.*, *Nucl. Instrum. Methods Phys. Res. A* **488**, 51 (2002).
 - [6] M. Bazzi *et al.*, *Phys. Lett. B* **704**, 113 (2011).
 - [7] A. Cieply, M. Mai, U.-G. Meißner, and J. Smejkal, *Nucl. Phys. A* **954**, 17 (2016).
 - [8] D. Sadasivan *et al.*, *Front. Phys.* **11**, 1139236 (2023).
 - [9] R. H. Dalitz and S. F. Tuan, *Phys. Rev. Lett.* **2**, 425 (1959).
 - [10] R. H. Dalitz and S. F. Tuan, *Ann. Phys.* **10**, 307 (1960).
 - [11] J. A. Oller and U.-G. Meißner, *Phys. Lett. B* **500**, 263 (2001).
 - [12] Y. Ikeda, T. Hyodo, and W. Weise, *Nucl. Phys. A* **881**, 98 (2012).
 - [13] Z. H. Guo and J. A. Oller, *Phys. Rev. C* **87**, 035202 (2013).
 - [14] M. Mai and U.-G. Meißner, *Eur. Phys. J. A* **51**, 30 (2015).
 - [15] A. Feijoo, V. Magas, and A. Ramos, *Phys. Rev. C* **99**, 035211 (2019).
 - [16] J.-X. Lu, L.-S. Geng, M. Doering, and M. Mai, *Phys. Rev. Lett.* **130**, 071902 (2023).
 - [17] T. Hyodo and D. Jido, *Prog. Part. Nucl. Phys.* **67**, 55 (2012).
 - [18] M. Mai, *Eur. Phys. J. Spec. Top.* **230**, 1593 (2021).
 - [19] D. W. Thomas *et al.*, *Nucl. Phys. B* **56**, 15 (1973).
 - [20] R. J. Hemingway, *Nucl. Phys. B* **253**, 742 (1985).
 - [21] I. Zychor *et al.*, *Phys. Lett. B* **660**, 167 (2008).
 - [22] K. Moriya and R. Schumacher (CLAS Collaboration), *AIP Conf. Proc.* **1441**, 296 (2012).
 - [23] G. Agakishiev *et al.* (HADES Collaboration), *Phys. Rev. C* **87**, 025201 (2013).
 - [24] R. Aaij *et al.* (LHCb Collaboration), *Phys. Rev. Lett.* **115**, 072001 (2015).
 - [25] R. Aaij *et al.* (LHCb Collaboration), *Phys. Rev. Lett.* **122**, 222001 (2019).
 - [26] M. Ablikim *et al.* (BESIII Collaboration), *Phys. Rev. Lett.* **110**, 252001 (2013).
 - [27] S. K. Choi *et al.* (Belle Collaboration), *Phys. Rev. Lett.* **91**, 262001 (2003).
 - [28] J. J. Wu, R. Molina, E. Oset, and B. S. Zou, *Phys. Rev. Lett.* **105**, 232001 (2010).
 - [29] L. Roca, J. Nieves, and E. Oset, *Phys. Rev. D* **92**, 094003 (2015).
 - [30] H. X. Chen, L. S. Geng, W. H. Liang, E. Oset, E. Wang, and J. J. Xie, *Phys. Rev. C* **93**, 065203 (2016).
 - [31] A. Esposito, L. Maiani, A. Pilloni, A. D. Polosa, and V. Riquer, *Phys. Rev. D* **105**, L031503 (2022).
 - [32] F.-K. Guo, C. Hanhart, U.-G. Meißner, Q. Wang, Q. Zhao, and B. S. Zou, *Rev. Mod. Phys.* **90**, 015004 (2018).
 - [33] A. Ramos, A. Feijoo, Q. Llorens, and G. Montaña, *Few-Body Syst.* **61**, 34 (2020).
 - [34] R. Aaij *et al.*, LHCb Collaboration, *Nat. Commun.* **13**, 3351 (2022).
 - [35] J. M. M. Hall, W. Kamleh, D. B. Leinweber, B. J. Menadue, B. J. Owen, A. W. Thomas, and R. D. Young, *Phys. Rev. Lett.* **114**, 132002 (2015).
 - [36] Z. W. Liu, J. M. M. Hall, D. B. Leinweber, A. W. Thomas, and J. J. Wu, *Phys. Rev. D* **95**, 014506 (2017).
 - [37] R. Molina and M. Döring, *Phys. Rev. D* **94**, 056010 (2016).

- [38] M. Lage, U.-G. Meißner, and A. Rusetsky, *Phys. Lett. B* **681**, 439 (2009).
- [39] K. Murakami, Y. Akahoshi, and S. Aoki, *Progr. Theor. Exp. Phys.* **2020**, 093B03 (2020).
- [40] N. Ishii *et al.*, *EPJ Web Conf.* **175**, 05013 (2018).
- [41] C. Drischler, *Prog. Part. Nucl. Phys.* **121**, 103888 (2021).
- [42] V. Metag, M. Nanova, and E. Ya. Paryev, *Prog. Part. Nucl. Phys.* **97**, 199 (2017).
- [43] N. Barnea, E. Friedman, and A. Gal, *Nucl. Phys. A* **968**, 35 (2017).
- [44] P. Adlarson *et al.*, *Phys. Rev. C* **102**, 044322 (2020).
- [45] P. Adlarson *et al.*, *Phys. Lett. B* **802**, 135205 (2020).
- [46] P. Adlarson *et al.*, *Nucl. Phys. A* **959**, 102 (2017).
- [47] Y. Tanaka *et al.*, *Phys. Rev. C* **97**, 015202 (2018).
- [48] S. D. Bass and P. Moskal, *Rev. Mod. Phys.* **91**, 015003 (2019).
- [49] M. Agnello *et al.*, *Phys. Rev. Lett.* **94**, 212303 (2005).
- [50] T. Yamazaki *et al.*, *Phys. Rev. Lett.* **104**, 132502 (2010).
- [51] G. Agakishiev *et al.*, *Phys. Lett. B* **742**, 242 (2015).
- [52] T. Yamaga *et al.*, *Phys. Rev. C* **102**, 044002 (2020).
- [53] F. Sakuma *et al.*, *Few-Body Syst.* **62**, 103 (2021).
- [54] S. Marri and J. Esmaili, *Eur. Phys. J. A* **55**, 43 (2019).
- [55] A. Gal, *Nucl. Phys. A* **914**, 270 (2013).
- [56] T. Sekihara, E. Oset, and A. Ramos, *Progr. Theor. Exp. Phys.* **2016**, 123D03 (2016).
- [57] T. Nagae, *Nucl. Phys. A* **954**, 94 (2016).
- [58] Y. Sada *et al.* (J-PARC E15 Collaboration), *Progr. Theor. Exp. Phys.* **2016**, 051D01 (2016).
- [59] S. Ajimura *et al.* (J-PARC E15 Collaboration), *Phys. Lett. B* **789**, 620 (2019).
- [60] O. Vazquez Doce *et al.*, *Phys. Lett. B* **758**, 134 (2016).
- [61] R. Del Grande *et al.*, *Eur. Phys. J. C* **79**, 190 (2019).
- [62] Y. Akaishi and T. Yamazaki, *Phys. Lett. B* **774**, 522 (2017).
- [63] J. Hrtankova, N. Barnea, E. Friedman, A. Gal, J. Mares, and M. Schafer, *Phys. Lett. B* **785**, 90 (2018).
- [64] M. Merafina, F. G. Saturni, C. Curceanu, R. Del Grande, and K. Piscicchia, *Phys. Rev. D* **102**, 083015 (2020).
- [65] T. Song, L. Tolos, J. Wirth, J. Aichelin, and E. Bratkovskaya, *Phys. Rev. C* **103**, 044901 (2021).
- [66] P. Senger, *Particles* **5**, 21 (2022).
- [67] H. Wolter *et al.*, *Prog. Part. Nucl. Phys.* **125**, 103962 (2022).
- [68] S. Hunt *et al.*, *Nature (London)* **606**, 276 (2022).
- [69] L. Tolos and L. Fabbietti, *Prog. Part. Nucl. Phys.* **112**, 103770 (2020).
- [70] D. B. Kaplan and A. E. Nelson, *Phys. Lett. B* **175**, 57 (1986).
- [71] T. Malik, S. Banik, and D. Bandyopadhyay, *Astrophys. J.* **910**, 96 (2021).
- [72] T. Muto, T. Maruyama, and T. Tatsumi, *Phys. Lett. B* **820**, 136587 (2021).
- [73] V. B. Thapa, M. Sinha, J. J. Li, and A. Sedrakian, *Phys. Rev. D* **103**, 063004 (2021).
- [74] A. Ramos and E. Oset, *Nucl. Phys. A* **671**, 481 (2000).
- [75] L. Tolos, D. Cabrera, and A. Ramos, *Phys. Rev. C* **78**, 045205 (2008).
- [76] D. Cabrera, L. Tolos, J. Aichelin, and E. Bratkovskaya, *Phys. Rev. C* **90**, 055207 (2014).
- [77] G. Raaijmakers, T. E. Riley, A. L. Watts, S. K. Greif, S. M. Morsink, K. Hebeler, A. Schwenk, T. Hinderer, S. Nissanke *et al.*, *Astrophys. J. Lett.* **887**, L22 (2019).
- [78] M. C. Miller *et al.*, *Astrophys. J. Lett.* **918**, L28 (2021).
- [79] T. E. Riley *et al.*, *Astrophys. J. Lett.* **918**, L27 (2021).
- [80] M. Adinolfi *et al.*, *Nucl. Instrum. Methods Phys. Res. A* **482**, 364 (2002).
- [81] J. Beringer *et al.* (Particle Data Group), *Phys. Rev. D* **86**, 010001 (2012).
- [82] C. Curceanu, K. Piscicchia *et al.*, *Acta Phys. Pol. B* **46**, 203 (2015).
- [83] F. Ambrosino *et al.*, *Nucl. Instrum. Methods Phys. Res. A* **534**, 403 (2004).
- [84] R. Del Grande, K. Piscicchia, and S. Wycech, *Acta Phys. Pol. B* **48**, 1881 (2017).
- [85] K. Piscicchia, S. Wycech, and C. Curceanu, *Nucl. Phys. A* **954**, 75 (2016).
- [86] K. Piscicchia *et al.*, *Phys. Lett. B* **782**, 339 (2018).
- [87] F. James and M. Roos, *Comput. Phys. Commun.* **10**, 343 (1975); F. James and M. Winkler, Report No. CERNLIB-D506, (CERN Program Library, 1994); C++ MINUIT User's Guide (2004).